NASA-TM-111601

AIAA

AIAA-96-1935
Blunt Body Near Wake Flow Field at Mach 6

Thomas J. Horvath and Catherine B. McGinley
NASA Langley Research Center
Hampton, VA

Klaus Hannemann
DLR
Gottingen, FRG

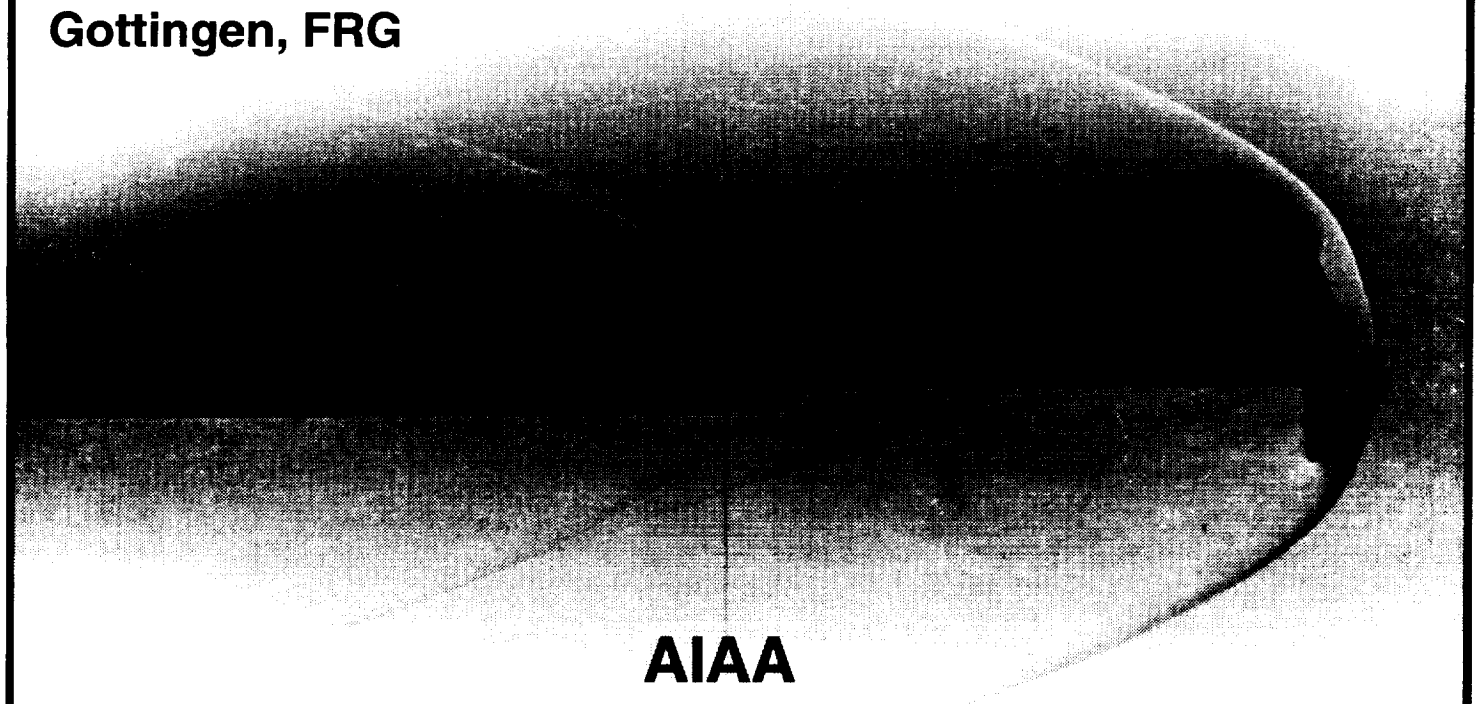

AIAA
27th Fluid Dynamics Conference
June 17-20, 1996 / New Orleans, LA

BLUNT BODY NEAR-WAKE FLOW FIELD AT MACH 6

Thomas J. Horvath Catherine B. McGinley
NASA Langley Research Center
Hampton, VA 23681

and

Klaus Hannemann
DLR, Institute of Fluid Mechanics
Gottingen, FRG

Presented at the
27th AIAA Fluid Dynamics Conference
June 18-20, 1996
New Orleans, LA

BLUNT BODY NEAR-WAKE FLOW FIELD AT MACH 6

Thomas J. Horvath Catherine B. McGinley
NASA Langley Research Center
Hampton, VA 23681

and

Klaus Hannemann
DLR, Institute of Fluid Mechanics
Gottingen, FRG

Abstract

Tests were conducted in a Mach 6 flow to examine the reattachment process of an axisymmetric free shear layer associated with the near wake of a 70 deg half angle, spherically blunted cone with a cylindrical after body . Model angle of incidence was fixed at 0 deg and free-stream Reynolds numbers based on body diameter ranged from $0.5x10^6$ to $4x10^6$. The sensitivity of wake shear layer transition on reattachment heating was investigated. The present perfect gas study was designed to compliment results obtained previously in facilities capable of producing real gas effects. The instrumented blunted cone model was designed primarily for testing in high enthalpy hypervelocity shock tunnels in both this country and abroad but was amenable for testing in conventional hypersonic blowdown wind tunnels as well. Surface heating rates were inferred from temperature - time histories from coaxial surface thermocouples on the model forebody and thin film resistance gages along the model base and cylindrical after body. General flow feature (bow shock, wake shear layer, and recompression shock) locations were visually identified by schlieren photography. Mean shear layer position and growth were determined from intrusive pitot pressure surveys. In addition, wake surveys with a constant temperature hot-wire anemometer were utilized to qualitatively characterize the state of the shear layer prior to reattachment. Experimental results were compared to laminar perfect gas predictions provided by a 3-D Navier Stokes code (NSHYP).

Shear layer impingement on the instrumented cylindrical after body resulted in a localized heating maximum that was 21 to 29 percent of the forebody stagnation point heating. Peak heating resulting from the reattaching shear layer was found to be a factor of 2 higher than laminar predictions, which suggested a transitional shear layer. Schlieren flow visualization and fluctuating voltage time histories and spectra from the hot wire surveys across the shear layer substantiate this observation. The sensitivity of surface heating to forebody roughness was characterized for a reattaching shear layer. For example, at $Re_{\infty,d} = 4x10^6$, when the shear layer was transitional, the magnitude of peak heating from shear layer impingement was reduced by approximately 24 percent when transition grit was applied to the forebody. The spatial location of the local peak, however, remained unchanged.

Nomenclature

C_h	Stanton number, $q_w / [r_\infty u_\infty (rh_t - h_w)]$
d	diameter, (in.)
d	boundary layer thickness, mm
h	enthalpy, (J/kg)
k	nominal roughness diameter, (mm)
M_∞	free stream Mach number
$p_{t,1}$	tunnel stagnation pressure, N/m^2
$p_{t,2}$	free stream pitot pressure, N/m^2
r	wall recovery factor
R	radius, (in.)
S	distance along model surface
t	time, (sec)
Re_∞	unit free stream Reynolds number, (m^{-1})
T	temperature, (K)
u	velocity, (m/sec)
x	axial distance from model base

Subscripts

∞	free-stream conditions
j	juncture
m	model forebody
n	model nose
ref	laminar reference heating
s	sting
stag	reference heating
t	reservoir stagnation conditions
w	wall

Introduction

NASA has examined the concept of aerobraking to satisfy planetary mission requirements. Aerobraking as defined by Jones, 1987, involves the use of aerodynamic forces acting on a spacecraft surface to decelerate. One proposed application of this technique for a planetary mission would be the placement of a science payload (Tauber et al, 1993; Mitcheltree, 1994) on or into the surface following a direct entry from an interplanetary flight.

One concept of this type, shown in Fig. 1, envisioned the use of a blunt umbrella shaped forebody to provide the aerobraking surface. The spacecraft design for a planetary direct entry approach can be similar. In this mission scenario, the desired payload and/or instrumentation package to be delivered to the surface would be placed behind the aerobrake to protect it from the intense heat generated during atmospheric entry. The Mars Pathfinder and Mars 98 missions under the NASA Discovery Program are examples of future planned missions utilizing this type of technology.

The accurate prediction of the near wake flow structure associated with blunt aerobrake concepts is an essential part of the design process as payload constraints are often imposed by wake closure. Proper positioning of the payload will be critical to insuring aerodynamic stability of the spacecraft during entry and to avoid thermal damage from localized near wake phenomenon. Although it is generally recognized that convective heating rates in the base region are low (Gnoffo, 1992), localized maxima can occur if the free shear layer that separates from the corner of the aerobraking surface (forebody) impinges on the after body (Gnoffo, 1992; Wells, 1990; Dye, 1993). The successful design of an aerobraking vehicle therefore requires an understanding of the physics associated with hypersonic, blunt-body, near-wake flowfields.

Understanding the physical aspects of the compressible free shear layer is of general interest as it can also be found in other practical situations. For example, internal flows involving axial flow combustors (King et. al., 1990; Herrin, 1995) often result in wake shear layers that are produced by fuel injectors. The growth and stability of these shear layers has a direct impact on the fuel-air mixing efficiency in scramjet combustors (e.g. Macaraeg, 1991).

The subject of near wake flows and free shear layers in relation to multiple conventional anti-armor projectiles in flight is briefly discussed by Herrin (1995). In his cited example, several of the fired missile projectiles are immersed in the near wake of the leading warhead (Hohler, 1990). In the context of aerodynamics, Herrin emphasizes the importance of understanding the wake flow physics in order to accurately define the flow conditions for the trailing bodies. From these few examples, it is evident that wake flows found in a variety of practical situations can give rise to a diverse range of complex fluid phenomenon ranging from flow unsteadiness, mixing, separation and flow reversal, to shear layer transition and/or reattachment.

Wake flows at supersonic and hypersonic speeds have been studied extensively both experimentally and theoretically since the 1950's. An in depth review of early work and discussions of wake characteristics is provided by Berger, 1971. In general, hypersonic near wake flows are characterized by several features which are schematically identified in Fig. 2. The inner or near wake flow consists of a recirculating fluid that is separated from the outer wake flow by a viscous shear layer that originates from the forebody boundary layer. A weak separation or "lip" shock may form as this boundary layer separates from the surface (Hama, 1966). As the opposing shear layers converge towards the rear stagnation point (in the absence of a solid surface), the flow is turned through a series of recompression waves which eventually coalesce into a recompression shock. Flow outside of the shear layer dividing

streamline continues downstream through a neck region; flow inside of the dividing streamline is turned back towards the base due to recompression. The addition of a solid surface will change the flow; but the salient features remain similar (Wells, 1990).

In 1992, a subgroup of an AGARD fluid dynamics panel (Working Group 18) was formed to address issues concerned with and related to blunt body wake flowfields. One of the stated experimental objectives of the ensuing activity was to examine real gas effects in the presence of a strongly expanded wake flow behind a 70° blunted cone. Non-intrusive flow diagnostics such as Planar Laser Induced Fluorescence (PLIF) or Laser Induced Fluorescence (LIF) of Nitrous Oxide (NO) were to be used to measure rotational temperature in the near wake. Surface measurements along the model forebody, base, and support sting were planned to help quantify blunt-body shear layer separation, turning angle, wake establishment/ unsteadiness, and wake closure in the presence of flows exhibiting real gas behavior. The experiments also were to help assess and quantify the performance of wind tunnels capable of producing real gas flows. The tests were to be conducted at a common test condition in several of the world's premiere hypervelocity shock tunnels: the piston-driven shock tunnel at DLR-Gottingen (HEG), the Large Energy National Tunnel (LENS) at Cubric/Calspan, and the 42-in, shock tunnel at NASA Ames (deactivated prior to tests). To date, non-intrusive measurements have been attempted at HEG but with very limited success (Rosenhauer, 1994). Fortunately, surface measurements made in these facilities have met with greater success and several continuum high-enthalpy experimental and computational studies have resulted (Kastell et. al., 1994, 1995; Holden, 1994; Holden et. al., 1995; Gochberg et al., 1996).

It was recognized within the AGARD 18 activity that along with real gas effects, shear layer transition to turbulence would have a first order influence on the near wake flow field, and in particular, the heating associated with reattachment. Furthermore, for a given test gas, the separation of these potential viscous effects from real gas effects would be difficult, if not impossible, to achieve from shock tunnel tests alone. A brief review of the relevant experimental literature on the subject of shear layer reattachment indicated that the peak heat transfer associated with an impinging transitional shear layer could be much higher than when the separated flow is entirely laminar or turbulent (Baker, 1966). Unfortunately, most blunt-body computational studies in the literature do not address the issue of shear layer transition but rather focus on forebody transition from laminar to turbulent flow prior to separation (Mitcheltree, 1995; Laurien, 1995). In an attempt to experimentally identify and separate wake viscous effects and wake flow establishment factors from potential real gas effects observed by Kastell and Horvath (1994), a set of tests (on the same model) was conducted at NASA Langley at Mach 10 and 6 in two conventional low enthalpy blowdown wind tunnels to compliment the high enthalpy, hypervelocity Mach 10 tests conducted at HEG and LENS.

The purpose of the conventional hypersonic tests at Langley was to obtain both flow field and surface measurements for a fully established wake flow in a well characterized free-stream. The objective of this paper is to present results from wake flow field surveys conducted in the NASA LaRC 20-Inch Mach 6 wind tunnel and to determine the state of the shear layer and to quantify its position and growth. Near wake surface heat transfer measurements are presented to evaluate viscous shear layer effects on reattachment heating. Measured heating distributions are compared to laminar Navier Stokes predictions.

Apparatus and Test

Model Description

A photograph and dimensioned sketch of the blunt cone model are shown in Figs. 3 and 4, respectively. The 6-in. diameter 70 deg blunted cone forebody was fabricated from Chromel rather than stainless steel to avoid the potential effects of extraneous EMF's resulting from the press-fit installation of Chromel-constantan coaxial surface thermocouples into a stainless steel model (Kidd, 1994; Wieting, 1987). The flat model base and 1.5-in. diameter cylindrical support sting were machined from conventional steel and slotted to accept instrumented ceramic (Macor) inserts. Quality assurance measurements on the model were made to

verify the accuracy of the surface geometry (±0.002 -in from nominal) and to precisely locate the individual sensors. The forebody was instrumented with 40 Chromel-constantan coaxial surface thermocouples along a single ray, while the base and sting ceramic inserts were instrumented with 65 thin film resistance gages as described by Miller (1981). Coaxial thermocouples were selected for use on the forebody because of their small size, fast response, and durability from particulate damage anticipated during the shock tunnel tests at HEG and NASA Ames.

For some of the tests, aluminum oxide grit of approximately 0.381 mm (0.015-in.) diameter was dispersed on the forebody stagnation region to examine the sensitivity of reattachment heating to surface roughness, Fig. 5. The ratio of nominal roughness diameter to computed boundary layer thickness was approximately 3 near the stagnation point and decreased to 1.2 at S/R_n = 0.9 (end of transition grit).

The uncooled model and support sting were attached to the facility support barrel approximately 2 model diameters downstream in an attempt to maintain setup consistency between all tests (HEG, LENS, and LaRC) performed on this model. Model angle of incidence was fixed at 0 deg. The entire assembly were injected to the tunnel centerline from a retracted position.

Facility Description

The model was tested in the 20-Inch Mach 6 Air Tunnel at the NASA Langley Research Center. A detailed description of this facility and related instrumentation is presented by Miller (1992). The 20-Inch Mach 6 is a blowdown facility which uses dried, heated, and filtered air as the test gas. Typical operating conditions for the tunnel are stagnation pressures ranging from 30 to 500 psia and stagnation temperatures from 76 to 1000 °R, yielding free stream unit Reynolds from 0.5 to $8x10^6$/ft. It has a closed 20-in by 20-in. test section with a contoured two-dimensional nozzle which provides a nominal free stream Mach number ranging from 5.8 to 6.1. A hydraulically operated model injection mechanism can inject the model into the flow in 0.5 seconds. A photograph of the test section, model, and support system arrangement are shown, Fig. 6. The maximum run time for this facility is approximately 5 minutes; typical run times for the separate wake surveys and heat transfer measurements for this test series were 180 and 5 seconds, respectively.

Mass flow and total temperature fluctuations of 2-3 percent and 1-1.5 percent, respectively, were measured previously by Stainback and Kubendran (1994) in the Mach 6 test section utilizing a dual wire constant temperature anemometer.

Instrumentation, Data Reduction, and Uncertainty

The reservoir pressure $p_{t,1}$ was measured with two silicon sensors having a full scale rating of 500 psia or 150 psia, depending on the operating condition of the tunnel. The reservoir temperature, $T_{t,1}$, was measured with two iron-constantan thermocouples inserted through the wall of the settling chamber. Test-section wall static and pitot pressures were monitored and compared to tunnel empty conditions to assess model blockage effects. Differences in pitot pressure of less than 0.5 percent were measured and it was concluded that significant blockage did not exist. The ratio of projected model frontal area-to- tunnel cross sectional area for the present test was 0.071. A 16-bit analog-to-digital acquisition system acquired the data on all channels at a rate of 50 samples per second except where noted.

Near wake pitot pressure was measured intrusively using a miniaturized (0.013-in, diameter tubing flattened on the probe tip) piezoresistive pressure transducer mounted to a wedge shaped water-cooled strut (Ashby, 1988) , as shown in Fig. 7. The close proximity of the transducer to the probe tip (approximately 3-in.) and a controlled thermal environment provided by the water-cooled housing jacket minimized pressure settling (lag) time and maintained a constant temperature at the transducer head during the traverse through the wake. Prior to a run, a sealed chamber placed over the assembly allowed the transducer to be calibrated in-situ. This daily in-situ calibration consisted of applying 13 known pressures selected to span the range of expected pressures and then applying a second order curve fit to the results. The defined pressure-voltage relationship was found to be

essentially linear. Pitot pressure was measured using a transducer rated for a maximum pressure of 20 psia to accommodate any unanticipated high pressures associated with the shear layer recompression process or tunnel unstart loads. During the traverse, the probe was stepped in increments of 0.003-in. with a dwell point at each position selected to allow the local pressure to settle. The probe position was determined from a known reference point on the model and the traverse stations (for both hot-wire and pitot surveys) preprogrammed prior to a run. While no attempt was made to correct for misalignments due to wind on loading during a run (model and survey support systems are independent), schlieren observations suggested little relative movement.

Schlieren videos (30 frames/sec) and still photographs (spark duration of 5nsec) were made of each run for visualization of the flow field. When necessary, digital enhancements of the schlieren images were performed using commercial software to bring out details of the near wake flow field.

A constant temperature hot wire anemometer was utilized to provide fluctuating voltage measurements and spectra to assess the state of the shear layer. The locations of the hot wire surveys were selected to correspond to the pitot measurement stations. Time histories of the instantaneous voltage fluctuations provided qualitative information regarding the distribution of r.m.s. energy. The constant temperature anemometer consisted of a 5 μm diameter Platinum-Rhodium wire operated at an overheat ratio of approximately 1 and sampled at 500 kHz. A more complete description of the acquisition system and analysis techniques can be found in Spina (1994).

Forebody surface temperature measurements were obtained using commercially available 0.031-in. diameter Chromel-constantan coaxial surface thermocouples that were press fit into the model wall. The model contoured junction was formed at the sensing surface by blending (lightly sanding) the two materials together. Several thermocouples had a second junction that was used to monitor the backside wall temperature in order to assess conduction effects. A general description of the coaxial thermocouple and its use is outlined by Kidd et. al. (1994).

The more sensitive thin film resistance gage was used to measure surface temperature in the base and wake regions. Standard mechanical deposition techniques developed at LaRC (Miller, 1981) were used to fabricate the 0.030-in. by 0.040-in. platinum sensing element. Surface temperatures were integrated over time to determine the local heat transfer rate using the computer code developed by Hollis (1995). Both analytical (Cook, 1970; Kendall-Dixon, 1967) and numerical finite-volume heat transfer models are incorporated into this code. The analytical solutions are derived from one-dimensional, semi-infinite solid heat conduction theory with the assumption of constant substrate (model) thermal properties. When using the analytical option the inferred heating rates are empirically corrected for the effects of variable model thermal properties. The finite-volume technique, which was used for the present tests, directly accounts for the variable model thermal properties (results from recent laboratory tests to determine substrate thermal properties have been incorporated into the code; Hollis, 1995). This option also removes the restriction of a semi-infinite wall boundary condition. This was an important consideration for this study as the model was designed and instrumented primarily for impulse facility testing where test times are on the order of milliseconds and the semi-infinite wall assumption is valid. In contrast, test times in the conventional hypersonic wind tunnels at LaRC were several orders of magnitude longer and led to invalidation of this assumption. For the present study, the uncertainty associated with variable wall thermal properties is believed to be minimal, particularly in the wake region where surface temperature increases of 30 °F or less were measured.

A typical temperature and C_h time history for a thin-film sensor located along the support sting in the wake region is shown in Fig.8. Unlike shock tunnel data where wake flow establishment times must be determined, the local Stanton number remains essentially constant upon reaching the tunnel centerline.

Measured values of $P_{t,1}$ and $T_{t,1}$ are believed to be accurate to within ±2 percent.

Based on manufacturer specifications, values of the near wake pitot pressure are estimated to be accurate to within ±5 percent. Based on previous experience, the accuracy of the heat transfer measurements is believed to be better than ±10 percent. Repeatability for the heat transfer measurements was found to be generally better than ±1 percent.

Computational method

The NSHYP code, used in the present study, was developed at DLR for the computation of supersonic and hypersonic flows of a perfect gas or a chemically reacting mixture of perfect gases (see Brenner et al., 1993, Brenner and Prinz, 1992, Riedelbauch and Brenner, 1990). Many hypersonic flow fields of interest permit the use of the thin-layer Navier-Stokes equations. However, due to the large recirculation region which develops in the wake of the blunted cone, the basic equations under consideration here are the full unsteady Navier-Stokes equations for a body-fitted coordinate system (x: streamwise, h: circumferential, z: wall normal coordinate),

$$\frac{\partial \hat{U}}{\partial t} + \frac{\partial \hat{E}}{\partial \xi} + \frac{\partial \hat{F}}{\partial \eta} + \frac{\partial \hat{G}}{\partial \zeta} = \frac{1}{\mathrm{Re}_{\infty,r}} \cdot \left[\frac{\partial \hat{E}_{vis}}{\partial \xi} + \frac{\partial \hat{F}_{vis}}{\partial \eta} + \frac{\partial \hat{G}_{vis}}{\partial \zeta} \right]$$

where

$$\hat{U} = J^{-1}\left(\rho, \rho u, \rho v, \rho w, e\right)^T$$

The inviscid and viscous fluxes are denoted by $\hat{E},\hat{F},\hat{G}$ and $\hat{E}_{vis},\hat{F}_{vis},\hat{G}_{vis}$ respectively. The transformed vector of the conservative variables is given by $\hat{U}$; here J^{-1} represents the jacobian of the transformation matrix. The equations have been nondimensionalized using the free stream density, velocity and viscosity and the radius of the blunted cone. For perfect gas computations the viscosity coefficient m and the coefficient of thermal conductivity k are calculated from the Sutherland law. The Prandtl number is assumed to be constant. The thermodynamic properties pressure and temperature are calculated from the conservative variables using the thermal and caloric state equation of perfect gas with the ratio of specific heats for diatomic gases (γ = 1.4).

The time discretization is fully implicit in order to avoid stiffness problems introduced by the small mesh increments in the boundary layer. NSHYP was primarily designed for the computation of steady flow fields. Therefore, the time integration was chosen to be of first order accuracy as only the converged steady-state solitions are of interest. The spatial derivatives of the inviscid fluxes are approximated by a second order upwind Total Variation Diminishing (TVD) formulation according to Yee and Harten (1987), and the spatial derivatives of the viscous fluxes are discretized by second order central differences. The TVD flux-difference splitting algorithm involves the solution of locally one-dimensional Riemann problems at the cell interfaces. Here the approximate Riemann solver of Roe (1981) is applied. Introducing a line Gauss-Seidel relaxation results in a linear system of block-tridiagonal matrices which is solved with the Richtmyer algorithm.

The physical domain considered here is bounded by the body, the inflow and outflow boundary and the line of symmetry. On the body no-slip conditions apply. The temperature of the isothermal wall is set to T_{wall} = 300K. The momentum equation in wall-normal direction is approximated by $\partial r/\partial n = 0$ at the wall. At the inflow boundary, a homogeneous supersonic flow is assumed. The free-stream conditions are given in Table 1. At the outflow boundary the conservative variables are extrapolated from the integration domain by assuming that their slope in the x-direction is constant, i.e. $d^2U/dx^2 = 0$. In order to compute axisymmetric flows with the present 3D code, appropriate symmetry conditions were employed to evaluate the fluxes in circumferential direction. At the line of symmetry, which for axisymmetric flows represents a singularity, the variables were determined by means of a cubic extrapolation.

Grid description and sensitivity studies will be deferred to the discussion of the comparisons of measurement with prediction.

Test conditions

Tests were performed at Mach 6 in air for nominal reservoir pressures and temperatures shown in Table 1. The nominal free stream

Reynolds numbers based on model diameter for these conditions were $0.5x10^6$, $2x10^6$, and $4x10^6$. A majority of the tests were conducted at $Re_{\infty,d} = 2x10^6$ (lower dynamic pressure) to minimize the chances of breaking the hot wire while maintaining high enough wake density gradients to visualize the separated shear layer via schlieren.

Results and Discussion

Approach

Initial tests were conducted on the blunted cone in the NASA LaRC 31-Inch Mach 10 Tunnel prior to the planned high enthalpy tests at HEG or LENS. These tests revealed the sensitivity of wake shear layer reattachment heating to Reynolds number, Fig. 9. The magnitude of the heating peak associated with reattachment is in the range of 16-18 percent of the measured forebody stagnation point heating These wake peak heating levels were also measured by Dye (1993) on a similar 70 deg sphere cone tested in the same facility. However, subsequent shock tunnel data (Holden, 1995) obtained on the present blunted cone configuration and corresponding laminar predictions from Moss (1995) imply that peak heating associated with laminar shear reattachment is typically 5-6 percent of the forebody stagnation point heating. One explanation for the differences observed between tests in the 31-Inch Mach 10 tunnel and LENS is that the relatively higher LaRC wake heating was produced by a non-laminar reattachment process.

The tests in the NASA LaRC 20-Inch Mach 6 Tunnel were initiated to provide both flow field and surface measurements to complement the Mach 10 results. The original objective of the experiment was to spatially locate the shear layer and define its growth via optical and intrusive measurements. The state (laminar/transitional/turbulent) of the shear layer and its influence on reattachment heating was to be determined using hot wire anemometry and surface heat transfer measurements, respectively. A condition was sought corresponding to a laminar shear layer. If a laminar condition was identified, shear layer transition would then be promoted using localized roughness placed on the forebody.

Based on similar magnitudes in the measured ratio of sting peak heating to forebody stagnation point heating from the present Mach 6 tests, a laminar condition was not identified. Because of this situation, CFD predictions were used to characterize laminar reattachment heating levels. The experimental measurements were used to establish the existence of a transitional/turbulent shear layer and to provide heating measurements for this type of reattachment process.

The data presented in the subsequent sections are organized and presented in the following manner: (1) Shear layer thickness vs. axial position are presented over the range of Reynolds numbers. (2) Surface heating distributions along the model forebody, base, and support sting are presented in the form of a normalized Stanton number, $C_h/C_{h,stag}$, where $C_{h,stag}$ corresponds to the measured stagnation point heating on the model forebody unless otherwise noted. (3) Hot wire fluctuating voltage time histories and spectra are highlighted to support the hypothesis that a transitional/turbulent shear layer exists prior to reattachment, and (4) Comparisons of measured heating with prediction along the forebody, base, and sting are made in the form of an unnormalized Stanton number, C_h.

Pitot pressure surveys

Near wake pitot pressure profiles were used to locate the mean shear layer boundaries. Based on schlieren photographs, several wake axial survey stations of interest were identified, Fig. 10. An example of a typical pitot pressure profile along a fixed axial station is shown, Fig. 11a. A schlieren photograph, Fig. 11b, illustrates the corresponding general flow features. As expected, the pressure decreases as the probe descends through the expansion fan. The small jump in the pressure near the trailing edge of the expansion fan corresponds to the lip shock discussed earlier (Hama, 1966). In this study, the boundary of the free shear layer is determined by the local slope change in the pitot pressure profile; visually, the shear layer can be seen in the schlieren image.

Shear layer boundaries inferred from a series of pressure profiles obtained along the wake axis are superimposed on a schlieren image obtained from a separate run, Fig. 12.

The close proximity of the mean shear layer boundaries determined via intrusive methods to that obtained optically, suggests that interference effects which could be expected from the survey strut and probe were not large. At low pressure conditions, where the density gradients were not sufficiently large enough to visualize the shear layer, these intrusive measurements were essential to properly locating the hot wire.

Shear layer thickness as a function of axial distance is generally linear as shown in Fig. 13. The measured shear layer thickness increases with decreasing Reynolds number.

Surface heating

Surface heating distributions obtained with and without forebody transition grit are shown over a range of Reynolds numbers, Fig. 14a-c. As expected for the smooth forebody, the heating in the stagnation region rapidly diminishes as the flow accelerates around the spherical nose. As the boundary layer expands and thins near the forebody shoulder the heating increases and then quickly falls off as the boundary layer separates from the base. On the model base low levels of heating are measured and further downstream a local peak occurs that is associated with the impingement of the shear layer on the sting.

The influence of roughness (via the transition grit) on the forebody and near wake heating is particularly evident at the two highest Reynolds numbers, Fig. 14b-c. From these data it is concluded that at the two highest Reynolds numbers ($Re_{\infty,d} = 2x10^6$ and $Re_{\infty,d} = 4x10^6$, the forebody boundary layer has transitioned to turbulent flow. The associated forebody heating has been augmented by up to a factor of two. This observation is consistent with flight calculations reported by Mitcheltree (1995) for laminar/turbulent forebody convective heating to a 70 deg blunted cone similar to the model tested. At $Re_{\infty,d} = 0.5x10^6$, Fig. 14a, the roughness was insufficient to promote a turbulent boundary layer and the forebody heating returned to nearly laminar levels as the flow expanded around the model shoulder.

The effect of Reynolds number on heating is shown, Fig. 15 a-b, for the smooth and rough models, respectively. In both situations, the heating peak associated with the near wake reattachment process increases in magnitude and moves towards the base with increasing Reynolds number. This behavior is indicative of a transitional/turbulent shear layer (Holden, 1995) (Berger, 1971).

Fig. 16 a-b presents the forebody heating distributions as measured on the rough model up to the point of separation on the model shoulder. The first data set, Fig. 16a, has been normalized by the measured stagnation point heating on the rough model. The second heating distribution, Fig. 16b, is the identical data normalized to the stagnation point heating as measured on the smooth model. The first format is selected to more clearly discuss trends, while the latter is selected to illustrate the apparent stagnation point heating augmentation due to the roughness located in the stagnation region. Fig. 16a indicates that the forebody boundary layer has transitioned to turbulence at S/R_n=0.4 with an associated heating maximum of approximately 35 percent above that measured at the stagnation point on the roughened model. The tripped heating distributions suggest a relaminarization of the boundary layer along the cone as it approaches the model shoulder at S/R_n = 2.1. The tripped flow found at the higher Reynolds numbers appears to have diminished the small local heating peak observed at the shoulder (S/R_n = 2.1) for laminar conditions, Fig. 15a. Noting this same trend in his turbulent flight calculations, Mitcheltree (1995) questioned the creditability of his turbulence model in this region of strong expansion. The present perfect gas data implies that the calculation of Mitcheltree in the shoulder region might be valid.

Fig. 16b normalizes the rough wall heating measurements to the smooth wall stagnation point heating. At the stagnation point, a heating augmentation of 17 percent above laminar levels at $Re_{\infty,d} = 4x10^6$ is noted. Holden (1983), reports several instances from wind tunnel and flight tests where boundary layer transition occurred in or just downstream of the stagnation region. In these examples cited by Holden, the stagnation point heating was found to be significantly larger than those predicted on the basis of laminar theory alone. He performed several studies to examine potential mechanisms which may have resulted in the enhanced stagnation heating. One study, involved trip rings placed 10 (or more)

boundary layer thicknesses downstream of the stagnation point. No significant heating increase at the stagnation point was measured. The roughness elements in the present study were placed immediately adjacent to the stagnation point (k/d = 3 at S/R_n = 0.05) and it is apparent that some form of influence is present for this situation.

Measured near wake heating distributions along the model base and sting over the range of Reynolds numbers with and without forebody transition grit are presented, Fig. 17a-b. The heating peak associated with the reattachment process is evident and occurs 1 to 1.3 model diameters (S/R_n = 7.8 to 8.8) downstream of the model base. Reattachment heating associated with the smooth model, Fig. 17b, indicate that the magnitude of the peak was approximately 21-29 percent of the measured forebody stagnation point suggesting a non laminar reattachment process. Tripping the forebody boundary layer tended to reduce the peak heating associated with reattachment, Fig. 17a. Similar to LaRC Mach 10 data on the same model, Fig. 9 and results presented by Hollis, (1995), an increase in Reynolds number produced an increase in magnitude and forward movement (towards the base) of the wake heating maximum.

Holden (1995) speculated that differences in measured wake heating levels from a broad range of AGARD 18 blunt-body tests could result from differences in the turbulent structure of the shear layer. As discussed earlier, Berger (1971) discussed several wake flow models that suggest the size of a laminar wake recirculation region should increase with increasing Reynolds number. The present Mach 6 wake heating trends imply that shear layer transition has occurred prior to reattachment/recompression. The heating on the model base remains below 6 percent of the stagnation level but is quite sensitive to Reynolds number. Complex recirculation regions have been noted in the present computations which may result in the local heating peaks that are measured on the model base. These results will be discussed in the Comparisons to Measurement section.

The influence of forebody transition grit on wake heating is summarized, Fig. 18. At $Re_{\infty,d} = 0.5x10^6$ there is no influence of the forebody roughness on the reattachment heating. The forebody heating distribution at this condition indicates boundary layer relaminarization prior to separation at the blunted cone shoulder. Based on the level of heating at reattachment, it is believed that the shear layer is transitional at the point of impingement on the sting. At $Re_{\infty,d} = 2x10^6$ and $4x10^6$ the peak heating measured on the sting was reduced by approximately 20 percent and 24 percent, respectively, when the forebody transition grit was applied. The spatial location of the heating maximum remained unchanged. Several repeat wind tunnel runs were to verify this trend: the experimental heating distributions were repeatable to within 1.1 percent. The forebody heating distribution at this condition indicates boundary layer transition has occurred prior to separation at the blunted cone shoulder. It is believed that at reattachment the free shear is turbulent.

These trends can be compared with supersonic heat transfer measurements made by Naysmith (1961) and later by Baker (1966) for reattaching flow over rearward facing steps. In these early studies, it was concluded that when transition from laminar to turbulent flow occurred along the separated shear layer, the peak heat transfer in the reattachment zone was much higher than when the shear layer was completely laminar or turbulent. The implication to the present results suggest that at a high enough Reynolds number, without the forebody transition grit, the instability mechanisms present (ie. tunnel noise, surface roughness etc.) were insufficient to produce a fully developed turbulent shear layer. The addition of surface roughness on the forebody may have been sufficient to promote a more developed turbulent shear layer which resulted in a heating reduction.

Hot wire surveys

To further clarify the state of the shear layer, an uncalibrated hot wire was traversed at stations corresponding to the pitot surveys. The intention was to try to detect laminar or turbulent signals in the shear layer and the data is strictly qualitative. Traverses were obtained at $Re_{\infty,d} = 0.5x10^6$ and $Re_{\infty,d} = 2x10^6$. A sequence of fluctuating voltage time histories obtained at $Re_{\infty,d} = 2x10^6$ and x/d = 0.333 for specific points within the shear layer is shown in Fig. 19a-d. Outside of the

shear layer Fig. 19a, the fluctuations are small. As the wire enters the shear layer, Fig. 19b, the signal becomes intermittent with occasional voltage drops which indicate times when the flow is decelerated. This behavior is consistent with turbulent signals when entering a shear layer. Toward the middle of the shear layer, Fig. 19c, the flow fluctuations increase in amplitude. As the wire departs the shear layer, Fig. 19d, headed toward the recirculating region, a pronounced intermittancy returns except now the voltage spikes are positive. Figure 20 shows the power spectra associated with trace (a) and (c) from the previous figure. The spikes in the data above 30kHz are from strain gauging and electronic noise and do not contribute substantially to the r.m.s levels. The spectra indicates that there is a spread of energy over a large frequency range. Furthermore, the energy in the middle of the shear layer is considerably larger than that outside the shear layer. These behaviors are characteristic of turbulent signals. Similar surveys were taken at x/d = 0.042, and 0.500. The data taken at x/d = 0.042 suggest that the flow is at least transitional at this station. All surveys indicate that the r.m.s voltage normalized by the mean voltage increases as the center of the shear layer is approached. Traveling downstream along the shear layer, the peak r.m.s levels increase quickly between x/d = 0.042 and x/d = 0.333 and then begin to level off between x/d = 0.333 and x/d = 0.500. This may be indicative of a shear layer completing the transition process. Hot wire data obtained at $Re_{\infty,d} = 0.5x10^6$ display similar trends but with much lower r.m.s levels.

Computational Predictions

Grid sensitivity

The computational results from the present study indicate the necessity of grid refinement studies to examine the sensitivity of the wake flow field and associated surface heating to grid spacing; particularly regarding blunt body base flow calculations. The topology of the nominal single block grid used in the present computations is shown, Fig. 21. In order to investigate the dependence of the solution on grid resolution, three grids containing 386x151, 193x76, and 97x38 points in wall tangential and wall normal direction, respectively, were used. The finest grid was first generated using the elliptic grid generator MEGACADS (Ronzheimer et. al. 1994) For this grid, the distance of the first grid line to the wall normalized to the radius of the forebody was $6x10^{-6}$. The remaining two grids were obtained by removing every second grid point in each direction.

The effect of the grid refinement on surface heating for $Re_{\infty,d} = 2x10^6$ are summarized in Fig. 22 a-b. All solutions obtained with the three grids were steady. As the comparisons of experimental data with prediction in this paper are limited to surface heat transfer, the discussion of grid convergence is restricted to the effect on heating distributions. The computed surface heat transfer along the forebody, Fig. 22a., showed little influence to grid refinement except at the stagnation point and on the model shoulder. The predicted heating at these two locations, however, was reduced with each successive refinement. For example, solutions obtained at these locations with the medium and fine grid agree to within 2 percent at the stagnation point and 8 percent at the model shoulder.

The predicted surface heating along the sting obtained with the three grid sizes, Fig. 22b, indicated that the heating peak associated with shear layer reattachment increased and moved slightly foreword towards the model base. Solutions obtained with the medium and fine grid show the magnitude of this heating peak remained essentially constant while the location was displaced 3 percent. Particle traces associated with the three grids, Fig. 23a-c, reveal the complexity of the predicted flow field found at the model base sting juncture. The particle traces shown were obtained by integration of the steady velocity field. Refinement of the grid appeared to resolve an additional fourth vortex within the base recirculation region (Fig. 23b-c). The reattachment point associated with the small vortex found just behind the model shoulder remained spatially fixed for all three grids.

In addition to the effects of grid refinement the sensitivity of surface heating to numerical damping was also investigated. The upwind TVD scheme which was used to perform the present computations requires an entropy correction to produce a numerically

stable solution. In this study, this form of artificial viscosity was varied from the maximum value permitted (see Yee, 1987) to the minimum value which still allowed a stable solution to be computed across the bow shock wave. The results from this investigation (not shown) indicated that the stagnation point heating obtained with the fine grid increased by 6 percent as the entropy correction parameter was reduced to its minimum value. At the same time, the localized heating peak found at the model shoulder decreased by approximately 6 percent. These percentages do not truly represent an expected uncertainty as the large numerical damping utilized in this parametric study are not routinely employed. The computed wake heating and base flow features were not affected as the artificial viscosity levels were varied.

Based on the present grid sensitivity study it has been concluded that accurate solutions have been achieved. The small differences in heating predicted between the medium and fine grid at the stagnation point and model shoulder are comparable to conclusions from a blunt body grid sensitivity study performed by Moss et. al. (1993). From an engineering perspective, the computed heating distribution obtained with the fine grid represents a conservative estimation. Extrapolation to finer meshes would yield lower predicted heating at the forebody stagnation point and shoulder. The magnitude of the shear layer reattachment heating peak on the sting did not change between solutions obtained with the medium and fine grids.

Comparisons to Measurement

Comparisons of predictions obtained with the fine mesh (386 x 151 grid) to measurements along the model forebody and base-support sting are shown in Figs. 24a-b, 25a-b, 26a-b, for $Re_{\infty,d}$ = $0.5x10^6$, $2x10^6$, and $4x10^6$ respectively. An unnormalized Stanton number was selected for comparative purposes as normalization can often mask differences between the distributions. On the forebody, Figs 24a, 25a, and 26a, the best agreement (less than 1.5 percent difference) was found along the cone section for $Re_{\infty,d}$ = $0.5x10^6$ and $Re_{\infty,d}$ = $2x10^6$. The largest disparity between measurement and laminar prediction on the cone section was 9 percent at $Re_{\infty,d}$ = $4x10^6$. At this higher Reynolds number it is possible the forebody boundary layer was approaching a transitional state. Although the measurements shown in Figs. 24a, 25a, and 26a were obtained without the use of transition grit, the particulate induced roughness on the model from the prior HEG shock tunnel tests may have been sufficient to promote a forebody boundary layer instability at $Re_{\infty,d}$ = $4x10^6$.

Spatial resolution of the heat transfer gages in the vicinity of the model shoulder was inadequate to resolve the local heat peak observed here computationally. The uncertainty of the measured heat transfer is greatest at the shoulder due to thermal conduction effects not accounted for in the data reduction process. The asymptotic behavior of the predicted heating as it nears the stagnation point of the spherical nose suggests that the finer, 386 x 151 grid was required to resolve the boundary layer and associated gradients. The use of this grid reduced the difference between stagnation point measurement and prediction to 2.3 percent at $Re_{\infty,d}$ = $4x10^6$.

The laminar calculations in the near wake indicated that the heating peak associated with reattachment was spatially located downstream of that inferred from measurement and was approximately 50 percent below the measured value in magnitude, Figs 24b, 25b, and 26b. This is consistent with the conclusions drawn earlier in this study. That is, for a transitional/turbulent reattaching shear layer, the size of the recirculation region is expected to diminish and the magnitude of the heating peak to increase relative to the laminar counterpart. The computed heating peak found downstream on the sting varied with Reynolds number and was 10-14 percent of the predicted forebody stagnation point heating. The corresponding experimental results varied from 21-29 percent.

Generally, the predicted base heating was twice that measured. It is assumed the local peak found on the base (S/R_n = 2.3) is the result of flow stagnation associated with the small vortex near the shoulder observed computationally, Fig. 23a-c. The predicted base heating associated with this flow structure was sensitive to Reynolds number and varied from 4-12 percent of the predicted forebody stagnation point heating. Validation of the complex recirculation patterns predicted

near the base-sting juncture were not possible as surface instrumentation was not placed in this location.

Concluding Remarks

The reattachment process of an axisymmetric free shear layer associated with the near wake of a blunt-body was experimentally and computationally investigated at Mach 6 over a free-stream Reynolds number range based on body diameter of 0.5×10^6 to 4×10^6. The configuration consisted of a 70 deg half angle, spherically blunted cone, with a cylindrical after body. Surface heating rates were computed from temperature-time histories from coaxial surface thermocouples on the model forebody and thin film resistance gages along the model base and cylindrical after body. The general flow features (bow shock, wake shear layer, and recompression shock) were visually identified by schlieren photography. Mean shear layer position and growth were determined from intrusive pitot pressure surveys. In addition, wake surveys with a constant temperature hot-wire anemometer were utilized to qualitatively characterize the state of the shear layer prior to reattachment. Perfect gas numerical simulations were provided by a 3-D Navier Stokes code (NSHYP).

Based on the present experimental results, the following conclusions can be made. Shear layer impingement on the instrumented cylindrical after body resulted in a localized heating maximum that was 21 to 29 percent of the forebody stagnation point heating. Peak heating resulting from the reattaching shear layer was found to be a factor of 2 higher than laminar predictions, suggesting a transitional or turbulent shear layer. An increase in Reynolds number produced an increase in magnitude and forward movement (towards the base) of the wake heating maximum on the sting; behavior indicative of a turbulent wake shear flow. Fluctuating voltage time histories and spectra from the hot wire surveys across the shear layer support this observation.

The sensitivity of surface heating to forebody roughness was characterized for a reattaching transitional shear layer. For example, at $Re_{\infty,d} = 4 \times 10^6$, when the shear layer was transitional, the magnitude of peak heating from shear layer impingement was reduced by approximately 24 percent when transition grit was applied to the forebody. The spatial location of the local peak, however, remained unchanged.

Acknowledgments

Without the assistance of the following individuals this work would not have been possible: Ed Self, Steve Parrish, Greg Draughon and Doug Grizzle for model fabrication / instrumentation support; Rhonda Manis, Grace Gleason, and Johnny Ellis for wind tunnel support; Bert Senter and Sheila Wright for data acquisition assistance; Dr. M. Sheplak for hot wire expertise; George Ashby for pitot pressure measurement assistance; Brian Hollis, Scott Berry, Brent Ross, and Dirk Kastell for data analysis support; and, Richard Wheless and Susan Bowen for documentation assistance. The authors gratefully acknowledge their contributions and behind the scenes work.

References

Ashby, George C. Jr. (1988) : Miniaturized Compact Water-Cooled Pitot-Pressure Probe for Flow-Field Surveys in Hypersonic Wind Tunnels. ISA 34th Int. Instr. Sym.

Baker, P.J.and Martin, B.W. (1966) : Heat Transfer in Supersonic Separated Flow Over A Two-Dimensional Backward-Facing Step. Int.J. Heat Mass Transfer, Vol. 9, p. 1081-1088.

Berger, Stanley A. (1971) : Laminar Wakes. American Elsevier Publ., Inc.

Brenner, G. and Prinz, U. (1992) : Numerical Simulation of Chemical and Thermal Nonequilibrium Flows after Compression Shocks. AIAA 27th Thermophysics Conference, July 6-8, Nashville, TN, AIAA 92-2879.

Brenner, G., Gerhold, T., Hannemann, K., and Rues, D. (1993) : Numerical Simulation of Shock/Shock and Shock-Wave/Boundary-Layer Interactions in Hypersonic Flows. Computers & Fluids, Vol. 22, No. 4/5.

Cook, William J. (1970) : Unsteady Heat Transfer Measurements to a Semi-Infinite Solid With Arbitrary Surface Temperature History and Variable Thermal Properties. Iowa State Univ. Tech Report ISU-ERI-AMES-67500.

Dye, T. P. (1993): An Experimental and Computational Investigation of the Flowfield About An Aeroassisted Space Transportation Vehicle at Mach 10. M. S. Thesis, University of Tennessee, Knoxville.

Gochberg, L.A., Allen, G.A., Gallis, M.A., and Deiwert, G.S. (1996) : Comparison of Computations and Experiments For Nonequilibrium Flow Expansions Around A Blunted Cone AIAA 34th Aerospace Sciences Meeting , Jan.15-18, Reno, NV., AIAA 96-0231

Gnoffo, P.A., Price, J.M., and Braun, R.D. (1992) : Computation of Near-Wake, Aerobrake Flowfields. J. Spacecraft and Rockets, Vol. 29, No.2.

Haas, B. L. and Venkatapathy, E. (1995) : Mars Pathfinder Computations Including Base-Heating Predictions. AIAA 30th Thermophysics Conference, June 19-22, San Diego, CA., AIAA 95-2086.

Hama, Francis A. (1966) : Experimental Investigations of Wedge Base Pressure and Lip Shock. Tech. Rep. No. 32-1033 (Contract No. NAS7-100), Jet Propulsion Lab., California Inst. of Technology.

Herrin, J.L. and Dutton, J.C. (1995) : The Turbulence Structure of A Reattaching Axisymmetric Supersonic Free Shear Layer. AIAA 26th Fluid Dynamics Conference, June 19-22, San Diego, CA., AIAA-95-2250.

Hohler, V. and Stilp, A. (1990) : Penetration Performance of Segmented Rods at Different Spacing- Comparison with Homogeneous Rods at 2.5-3.5 km/s. Proceedings of the 12th Int. Sym. on Ballistics, Vol. 78, No. 12.

Holden, M.S., Chadwick, K.M., Gallis, M.A., and Harvey, J.K.(1995): Comparison Between Shock Tunnel Measurements On A Planetary Probe Configuration and DSMC Predictions. Proceedings of the 20th Int. Sym. on Shock Waves, July 23-28, Pasadena, CA.

Hollis, Brian R. (1995) : User's Manual for the One-Dimensional Hypersonic Experimental Aero-Thermodynamic (1DHEAT) Data Reduction Code. NASA CR 4691, (Grant Nos. NAG1-1663, NAGW-1331).

Hollis, B.R. and Perkins, J.N.(1995) : Hypervelocity Aeroheating Measurements in Wake of Mars Mission Entry Vehicle. AIAA 26th Fluid Dynamics Conference, June 19-22, San Diego, CA., AIAA-95-2314.

Jones, Jim J. (1987) : The Rationale for an Aeroassist Flight Experiment. AIAA 22th Thermophysics Conference, June 8-10, Honolulu, HI., AIAA-87-1508.

Kastell, D., Horvath T.J., and Eitelberg G. (1994) : Nonequilibrium Flow Expansion Around a Blunted Cone. 2nd European Symposium on Aerothermodynamics for Space Vehicles. Norwijk, NL.

Kastell, D., Hannemann K., Eitelberg G., and Horvath T.J. (1995): Recompression of Nonequilibrium Flow in the Wake of a Blunted Cone. Proceedings of the 20th Int. Sym. on Shock Waves, July 23-28, Pasadena, CA.

Kendall, D.N., Dixon, W.P., and Schulte, E.H.(1967): Semiconductor Surface Thermocouples for Determining Heat-Transfer Rates. IEEE Transactions on Aerospace and Electronic Systems, Vol AES-3, No. 4.

Kidd, C.T., Nelson, C.G., and Scott, W.T. (1994).: Extraneous Thermoelectric EMF Effects Resulting From The Press-Fit Installation Of Coaxial Thermocouples in Metal Models. Proceedings of the 40th International Instrumentation Symposium, Baltimore, MD.

Laurien E. (1995) : Numerical Investigation of Laminar-Turbulent Transition in the Boundary-Layer of Reentry Capsules. AIAA 33rd Aerospace Sciences Meeting, January 9-12, Reno, NV., AIAA-95-0775.

Macaraeg,M. G., and Streett, C.L. (1991): Linear Stability of High-Speed Mixing Layers. Applied Numerical Mathematics, Vol.7.

Mitcheltree, Robert A. (1994) : Aerothermodynamic Methods for a Mars Environmental Survey Mars Entry. J. of Spacecraft and Rockets, Vol. 31, No. 3.

Mitcheltree, Robert A. (1995) : Computational Aerothermodynamics for Mars Pathfinder Including Turbulence. AIAA Atmospheric Flight Mechanics Conference, August 9, Baltimore, MD, AIAA-95-3493.

Miller, Charles G. III (1992) : Hypersonic Aerodynamic/Aerothermodynamic Testing Capabilities at Langley Research Center. AIAA 17th Aerospace Ground Testing Conference, July 6-8, Nashville, TN., AIAA-92-3937.

Miller, Charles G. III (1981) : Comparison of Thin-Film Resistance Heat-Transfer Gages With Thin-Skin Transient Calorimeter Gages in Conventional Hypersonic Wind Tunnels. NASA TM 83197.

Moss, J.N., Mitcheltree, R.A., and Wilmoth, R.G. (1993) : Hypersonic Blunt Body Wake Computations Using DSMC and Navier-Stokes Solvers. AIAA 28th Thermophysics Conference, July 6-9, Orlando, FL. AIAA-93-2807.

Moss, J.N., Price, J.M., and Dogra, V.K. (1995) : DSMC Calculations for a 70° Blunted Cone at 3.2 km/s in Nitrogen. NASA TM 109181.

Naysmith, A. (1961) : Measurements of Heat Transfer in Bubbles of Separated Flow in Supersonic Air Streams. ASME & Instn. Mech. Engrs., Int. Heat Transfer Conf., Part II, London.

Riedelbauch, S and Brenner, G. (1990) : Numerical Simulation of Laminar Hypersonic Flow Past Blunt Bodies Including High Temperature Effects. AIAA 21st Fluid Dynamics and Lasers Conference, Seattle, Washington, AIAA 90-1492.

Roe, P. L. (1981) : Approximate Riemann Solvers, Parameter Vectors, and Difference Schemes. J. Comp. Physics, Vol. 43, pp. 357-372.

Ronzheimer, A., Brodersen, O., Rudnik, R., Findling, A., and Rossow, C. (1994): A New Interactive Tool for the Management of Grid Generation Processes Around Arbitrary Configurations. 4th International Conference on Numerical Grid Generation in Computational Fluid Dynamics and Related Fields, Swansea UK, April 6-8.

Rosenhauer, M., Wollenhaupt, M., Scheer, M., and Beck, W.H. (1994) : LIF Measurements in the Wake of A Blunt Body In HEG. 2nd European Symposium on Aerothermodynamics for Space Vehicles. Norwijk, NL.

Spina, E.F. and McGinley, C. B. (1994) : Constant-Temperature Anemometry in Hypersonic Flow: Critical Issues and Sample Results. Experiments in Fluids, No.17.

Stainback, P.C. and Kubendran, L.R. (1994) The Measurement of Disturbance Levels in the Langley Research Center 20-Inch Mach 6 Tunnel. NASA CR 4571, NAS1-19320.

Tauber, M., et al (1993) : MESUR Probe Aerobrake Preliminary Design Study. J. Spacecraft and Rockets,Vol. 30, No.4 .

Thornton, Aimee D. (1993) : A Computational and Analytical Investigation of High Total-Enthalpy Supersonic Shear-Layer Data. MS Thesis, The George Washington University.

Wells, William L. (1990) : Surface Flow and Heating Distributions on a Cylinder in Near Wake of Aeroassist Flight Experiment (AFE) Configuration at Incidence in Mach 10 Air. NASA TP 2954.

Wieting, Allan R. (1987) : Experimental Study of Shock Wave Interference Heating on a Cylindrical leading Edge. NASA TM 100484.

Yee, H. C. and Harten, A. (1987) : Implicit TVD Schemes for Hyperbolic Conservation Laws in Curvilinear Coordinates. AIAA J., Vol. 25, pp. 266-274.

Table 1. Nominal Flow Conditions

$Re_{\infty,d}$	0.5×10^6	1×10^6	2×10^6	3.5×10^6
$P_{t,1}$ (N/m^2)	4.05×10^5	8.62×10^5	17.2×10^5	32.7×10^5
$T_{t,1}$ (°K)	493.7	508.8	505.0	523.9
r_∞ (kg/m^3)	1.68×10^{-2}	3.22×10^{-2}	6.45×10^{-2}	11.54×10^{-2}
T_∞ (°K)	63.3	63.4	62.7	64.4
u_∞ (m/sec)	931	947.6	943.8	962.2
M_∞	5.84	5.93	5.94	5.98

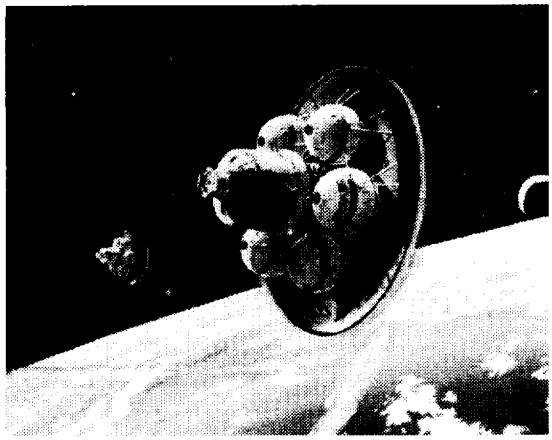

Fig. 1. Conceptual drawing of an aerobraking vehicle.

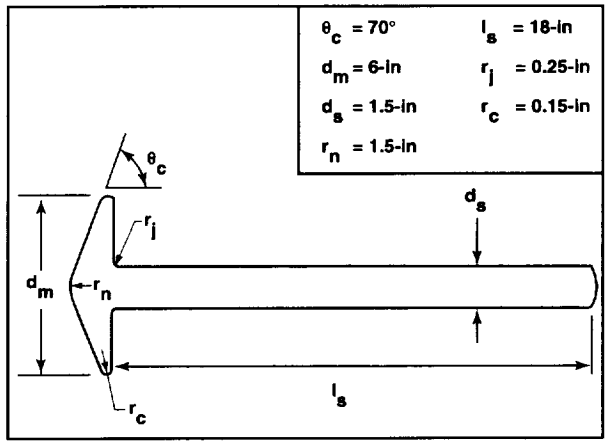

Fig. 4. Dimensional sketch of 70° blunted cone model.

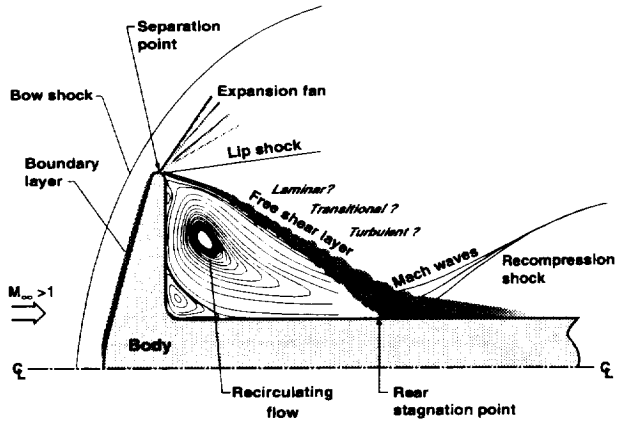

Fig. 2. Schematic representation of the base flow region behind a blunt body in hypersonic flow.

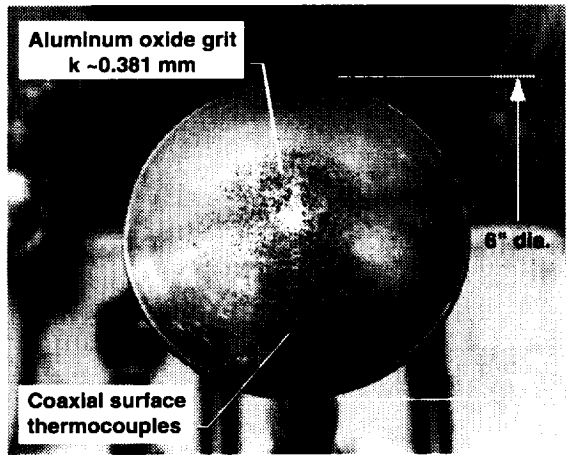

Fig. 5. Transition grit dispersed on blunted cone (front view).

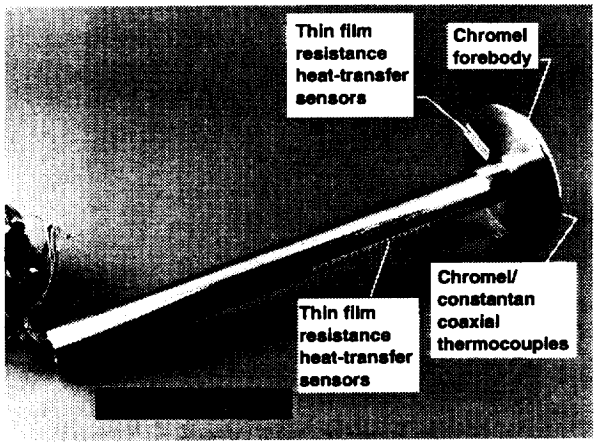

Fig. 3. Photograph of instrumented 70° blunted cone heat transfer model.

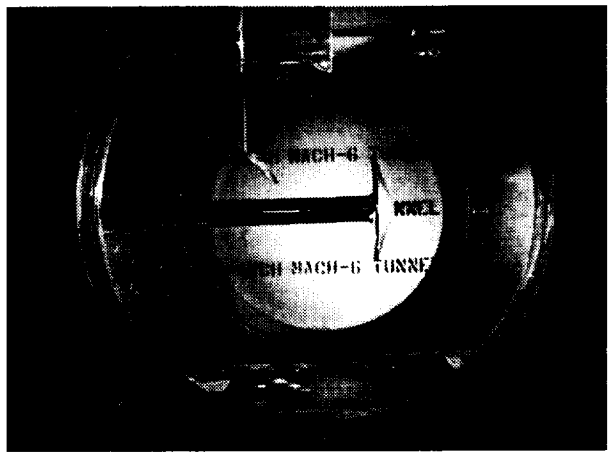

Fig. 6. Blunted cone and pitot survey system installed in LaRC 20-in. Mach 6 test section.

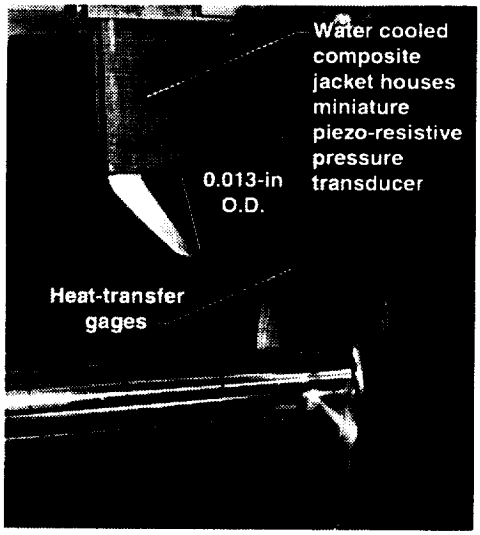

Fig. 7. Pitot survey assembly.

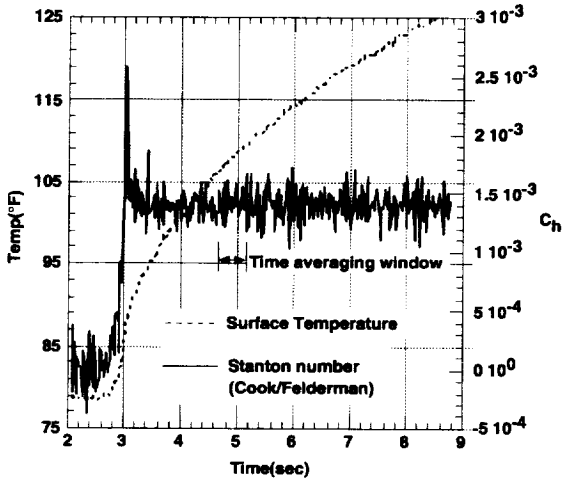

Fig. 8. Temperature and Stanton number time history for a wake thin film gage.

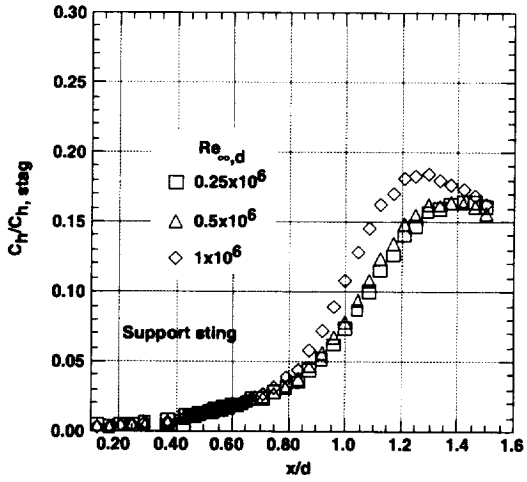

Fig. 9. Effect of Reynolds number on normalized sting stanton number heating distribution $M_\infty = 10$, smooth forebody.

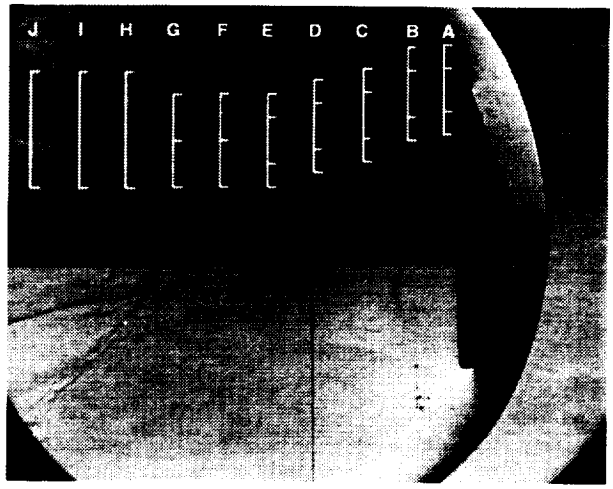

Fig. 10. Schlieren photograph indicating pitot pressure and hot wire axial survey stations. $M_\infty = 6$, $Re_{\infty,d} = 2x10^6$

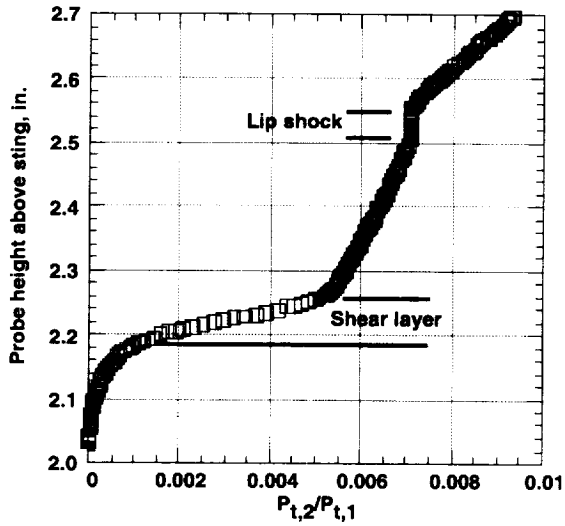

(a) Pitot traverse thru shear layer

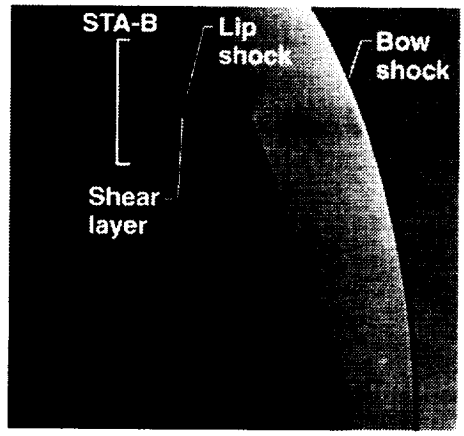

(b) Schlieren photograph

Fig. 11. Typical pitot pressure distribution and general flow features observed from blunt body near wake flowfield. $M_\infty = 6$, $Re_{\infty,d} = 2x10^6$ Sta. B

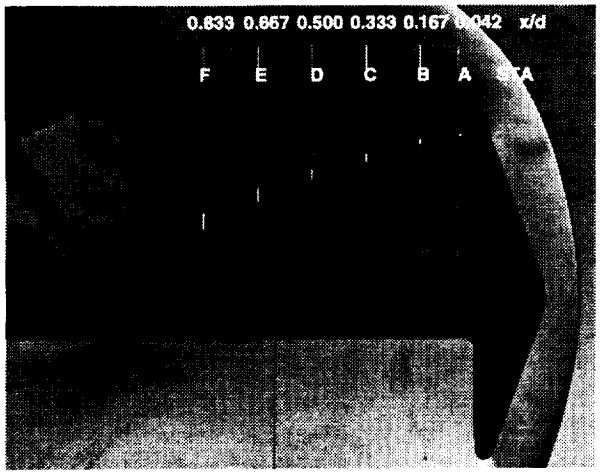

Fig. 12. Comparison of shear layer thickness inferred from pitot pressure surveys with schlieren image. $M_\infty = 6$, $Re_{\infty,\,d} = 4x10^6$

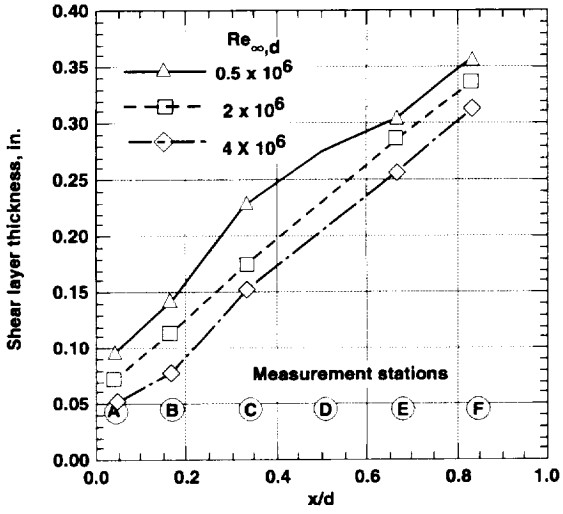

Fig. 13. Effect of Reynolds number on shear layer thickness as measured from wake pitot surveys. $M_\infty = 6$

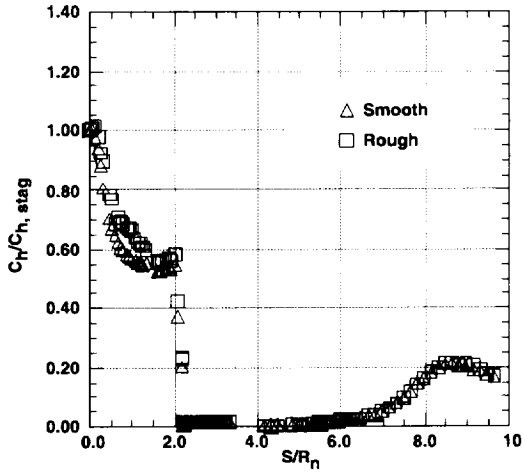

(a) $M_\infty = 6$, $Re_{\infty,\,d} = 0.5x10^6$ *(k ~0.381 mm)*

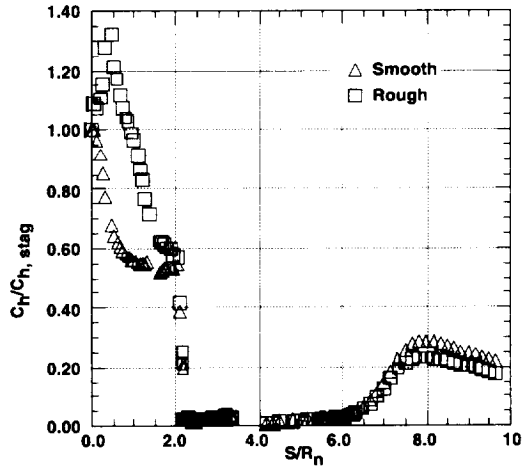

(b) $M_\infty = 6$, $Re_{\infty,\,d} = 2x10^6$ *(k ~0.381 mm)*

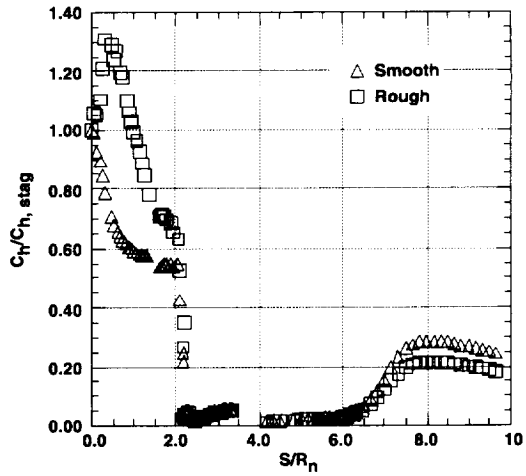

(c) $M_\infty = 6$, $Re_{\infty,\,d} = 4x10^6$ *(k ~0.381 mm)*

Fig. 14. Effect of forebody roughness on normalized Stanton number heating distribution.

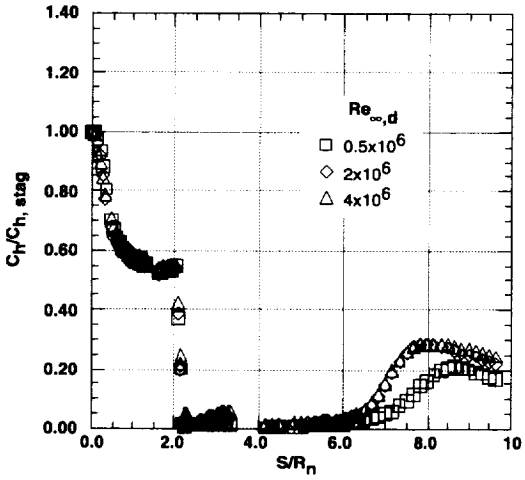

(a) $M_\infty = 6$, smooth forebody

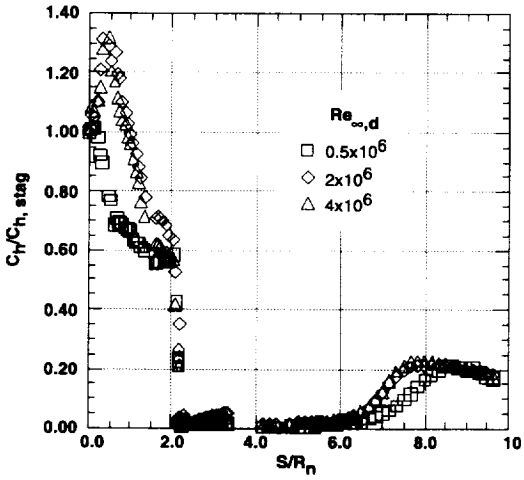

(b) $M_\infty = 6$, rough forebody ($k \sim 0.381$ mm)

Fig. 15. Effect of Reynolds number on normalized Stanton number heating distribution.

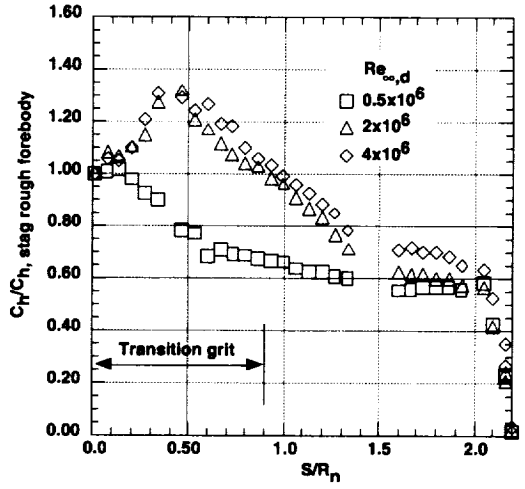

(a) $M_\infty = 6$, ($C_{h,\ stag}$ rough forebody) $k \sim 0.381$ mm

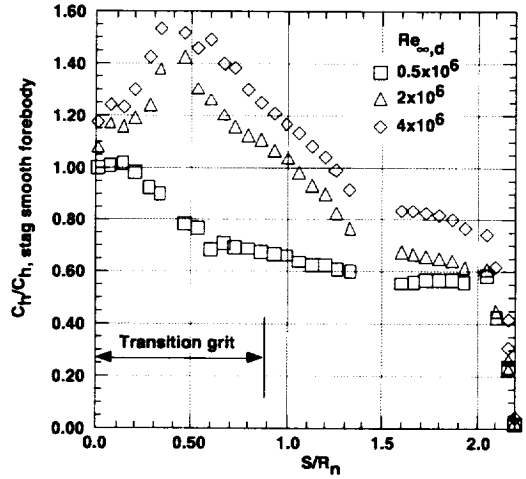

(b) $M_\infty = 6$, ($C_{h,\ stag}$ smooth forebody) $k \sim 0.381$ mm

Fig. 16. Effect of Reynolds number on normalized forebody Stanton number heating distribution.

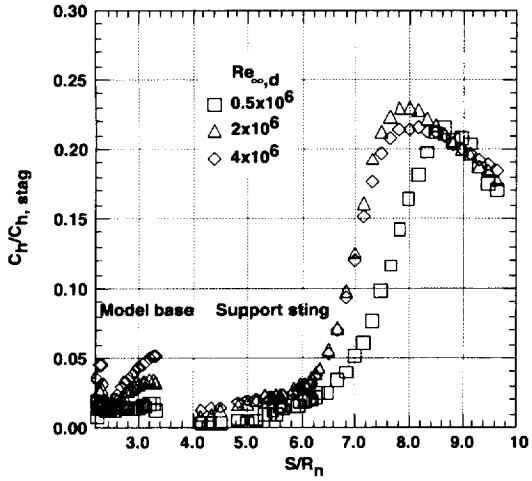

(a) $M_\infty = 6$, rough forebody ($k \sim 0.381$ mm)

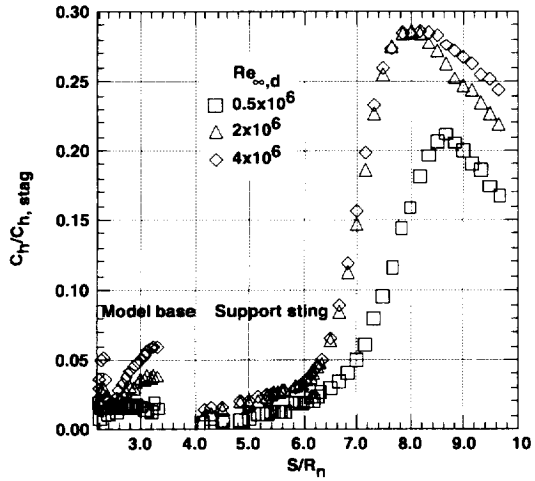

(b) $M_\infty = 6$, smooth forebody

Fig. 17. Effect of Reynolds number on normalized base/sting Stanton number heating distribution.

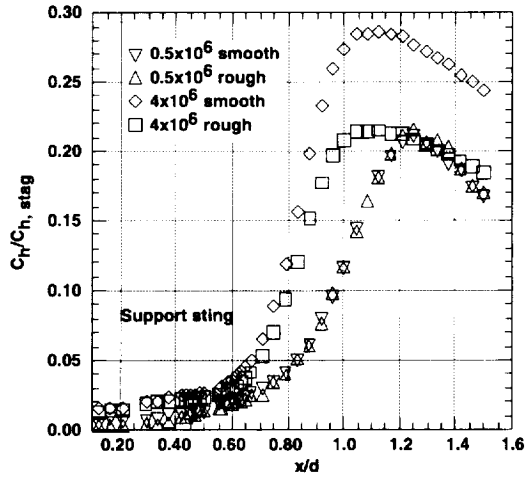

Fig. 18. Effect of forebody roughness on normalized sting Stanton number heating distribution. $M_\infty = 6$, ($k \sim 0.381$ mm)

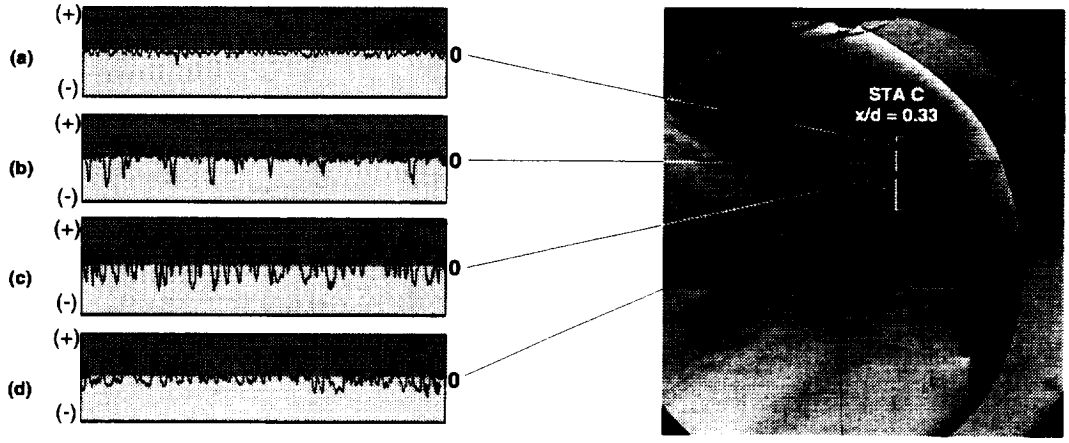

Fig. 19. Fluctuating voltage time histories during a typical hot wire traverse thru shear layer.

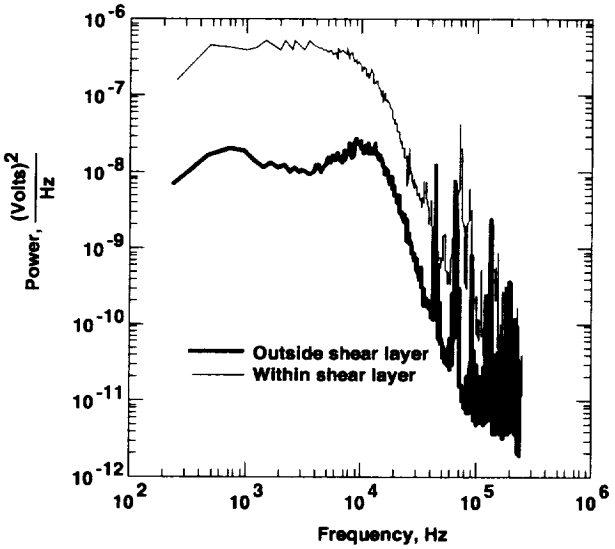

Fig 20. Power spectra outside and within the shear layer. M_∞ = 6, $Re_{\infty,d}$ = 2x10^6, x/d = 0.333, rough forebody

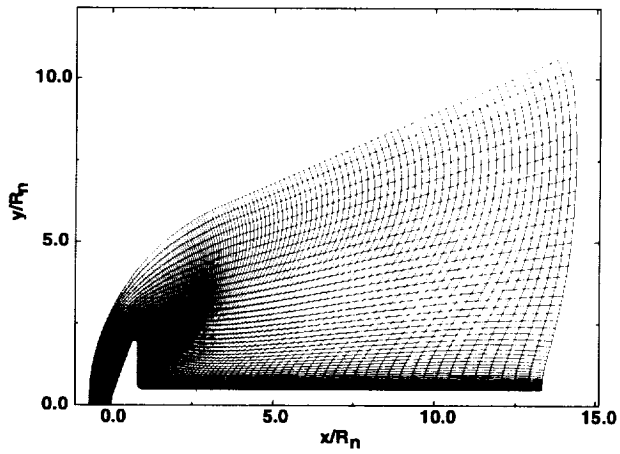

Fig 21. Computational grid for NS code simulation of blunt body flow. Mesh size 193 x 76.

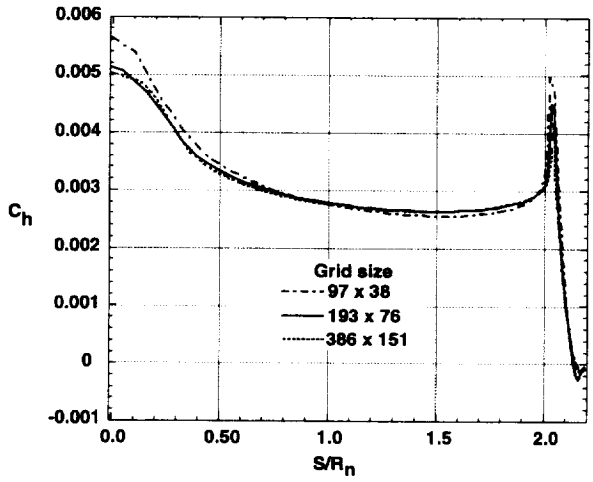

(a) Forebody

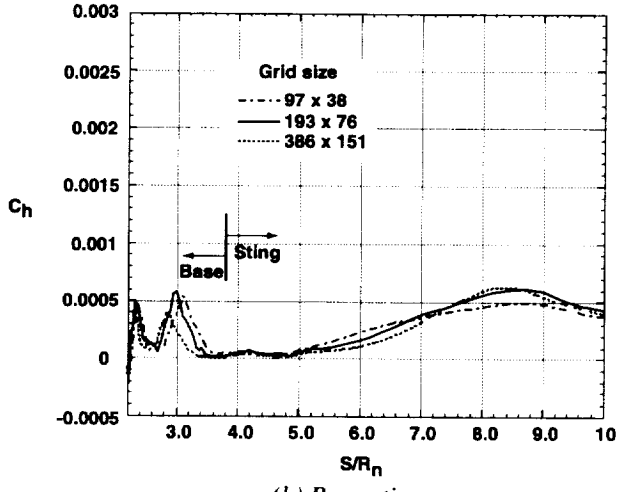

(b) Base-sting

Fig 22. Effect of grid refinement on predicted Stanton number heating distribution. M_∞ = 6, $Re_{\infty,d}$ = 2x10^6, laminar

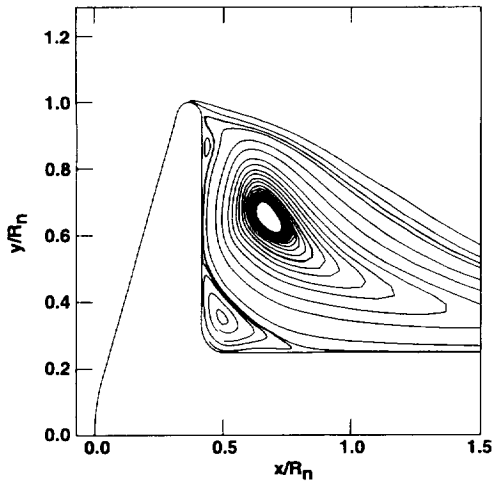

(a) Mesh size = 97 x 38

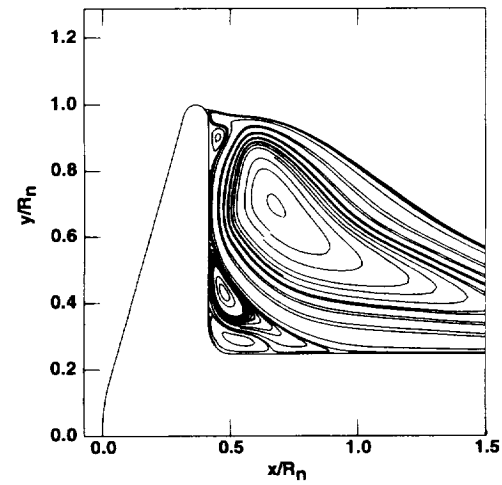

(b) Mesh size = 193 x 76

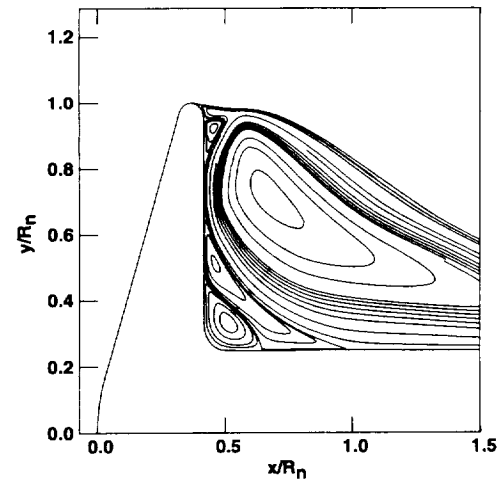

(c) Mesh size = 386 x 151

Fig 23. Particle paths for computational wake flowfield.
M_∞ = 6, $Re_{\infty,d}$ = 2x10^6, laminar

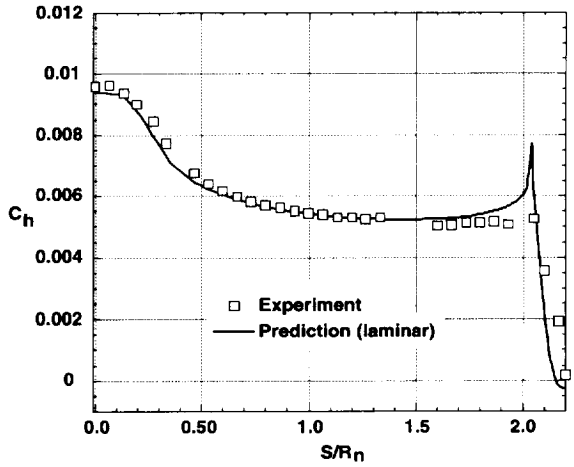

(a) Forebody

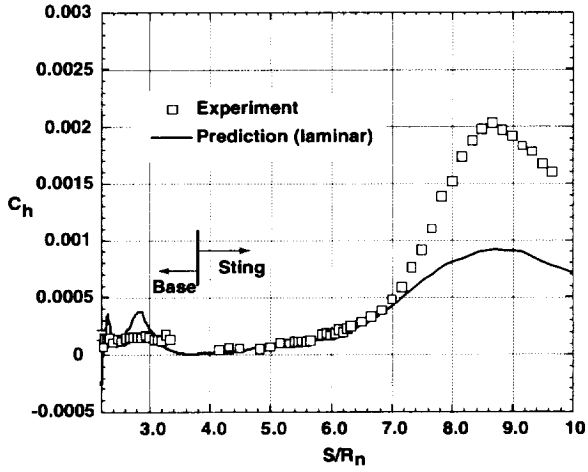

(b) Base-sting

Fig 24. Comparison of measured Stanton number heating distribution with prediction.
M_∞ = 6, $Re_{\infty,d}$ = 0.5x10^6

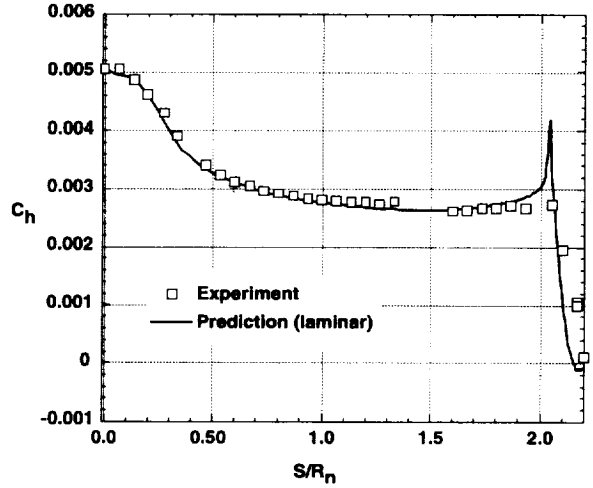

(a) Forebody

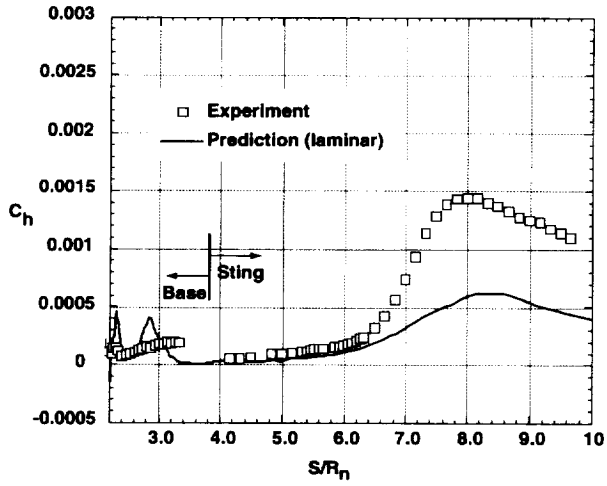

(b) Base-sting

Fig 25. Comparison of measured Stanton number heating distribution with prediction. $M_\infty = 6$, $Re_{\infty,d} = 2x10^6$, laminar

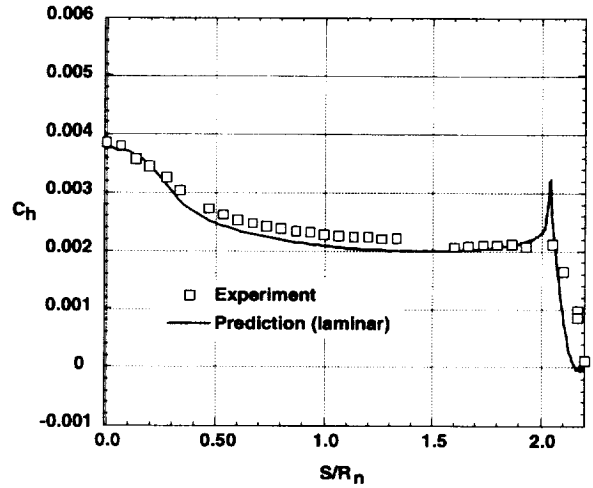

(a) Forebody

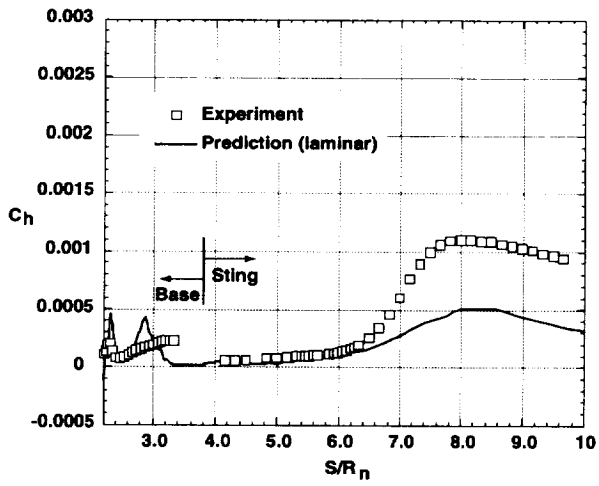

(b) Base-sting

Fig 26. Comparison of measured Stanton number heating distribution with prediction. $M_\infty = 6$, $Re_{\infty,d} = 4x10^6$